Fatigue Behavior of the Rare Earth Rich EV31A Mg Alloy: Influence of Plasma Electrolytic Oxidation

Lorella Ceschini[1], Alessandro Morri[1]*, Valerio Angelini[1], Simone Messieri[2]

[1] Department of Industrial Engineering (DIN), Alma Mater Studiorum – University of Bologna, Italy.
   lorella.ceschini@unibo.it, valerio.angelini4@unibo.it,

[2] Ducati Motor Holding – Bologna Italy. simone.messieri@ducati.com

* Correspondence: alessandro.morri@unibo.it; tel +39 0512093463; fax +39 0512093467

Abstract: Rare earth rich magnesium alloys are used in aerospace and automotive fields because of their high specific strength and good castability. However, due to their low corrosion resistance, protective surface treatments, such as conversion coating or electroless plating are necessary, when they have to be used in humid or corrosive environments. The present study was aimed to evaluate the effect of Plasma Electrolytic Oxidation (PEO) and different surface roughness   (Ra≈0.8 µm and Ra≈0.3 µm) on the rotating bending fatigue of an innovative Mg alloy, with a high content of Nd (up to 3.1 wt%) and Gd (up to 1.7 wt %). Fatigue tests revealed a 15% decrease in the fatigue strength of the PEO treated alloy (fatigue strength = 88 MPa) with respect to the bare alloy (fatigue strength = 103 MPa). The reduction of fatigue strength was mainly due to the residual tensile stresses induced by the PEO treatment. The effect of surface roughness on the bare alloy was, instead, negligible. The mechanisms of crack initiation were similar in the untreated and PEO treated alloy, with crack nucleation sites located in correspondence of large facets of the cleavage planes.

Keywords: Rare earth rich magnesium alloy, Plasma Electrolytic Oxidation, PEO, Microstructure, Fatigue

1. Introduction

Due to their low density, high specific strength, good vibrational absorption and good castability [1–4], Mg alloys are increasingly used in aerospace and automotive fields. Structural components for the transport industry, such as camshaft covers, clutch and transmission housings, intake manifolds, engine blocks, steering components, radiator supports, and automobile wheels, are inevitably subjected to cyclic stresses in service. For this reason, investigation on the fatigue behaviour of both cast and wrought Mg alloys has recently drawn considerable interest [5–9]. Recent studies [7,9,10] have demonstrated that the addition of rare earth (RE) elements, such as Nd, Gd, Y, can remarkably enhance both the tensile and fatigue strength of Mg alloys. In the case of castings, this improvement was related both to the microstructural refinement and to the decreased size and amount of porosity and inclusions induced by RE elements [7,11,12], while in wrought Mg alloys it seems mainly due to the corresponding weakness of crystallographic textures and the reduction of twinning [13–16]. It was also found that the addition of RE and the reduction of impurities can effectively improve the corrosion resistance of Mg alloys [17–20].

However, when components have to be used in humid or corrosive environments and/or improved wear resistance is needed, also Mg-RE alloys can be inadequate and protective surface treatments, such as conversion coating or electroplating/electroless plating are necessary [21–23].

Among the conversion coating processes, plasma electrolytic oxidation (PEO) is gaining increasing attention, since it is able to produce relatively thick, dense and protective surface oxide layers with enhanced wear and corrosion resistance [24–26]. Moreover, the lower residual surface stresses and amount of microstructural defects in the conversion layer, with respect to traditional oxide coating, seem to reduce its adverse effect on the fatigue properties of Mg alloys.

To date, however, few data on the fatigue behaviour of RE-containing cast Mg alloys are available [6,12,27–29] and also the effect of anodisation or PEO has been mainly investigated on traditional wrought Mg-alloys without RE addition [21–23,30].

Based on the above, the present study was aimed to evaluate the rotating bending fatigue behaviour of an innovative casting Mg alloy, with a high content of Nd (up to 3.1 wt%) and Gd (up to 1.7 wt%). The excellent fluidity of this alloy, thanks to the high amount of Nd, enables the production of sand cast components, with very low defect content and an average grain size comparable to that of wrought alloys. The effect of different surface roughness on the untreated alloy, as well as of surface modification by Plasma Electrolytic Oxidation (PEO), was evaluated.

2. Materials and Methods

The RE-rich magnesium alloy used in the present study was provided by Magnesium Elektron® and its chemical composition is reported in Table 1.

Table 1. Chemical composition (wt%) of Elektron 21® (EV31A) magnesium alloy. (Magnesium Elektron® test report).

Nd	Gd	Zr	Zn	Cu	Fe	Ni	Si	Mg
2.8	1.5	0.53	0.25	<0.008	<0.003	<0.001	<0.01	Bal.

Fatigue test samples were machined from sand castings to the final geometry reported in Fig. 1 according to ISO-1143 [31] and then were T6 heat treated according to standard conditions (solutionising at 520°C for 8 h; quenching in water at 70°C; and aging at 200°C for 16 h). These treatment conditions were defined on the basis of the results of a previous work, carried out by the authors, focused on the influence of heat treatment on microstructure and tensile strength of this alloy [34].
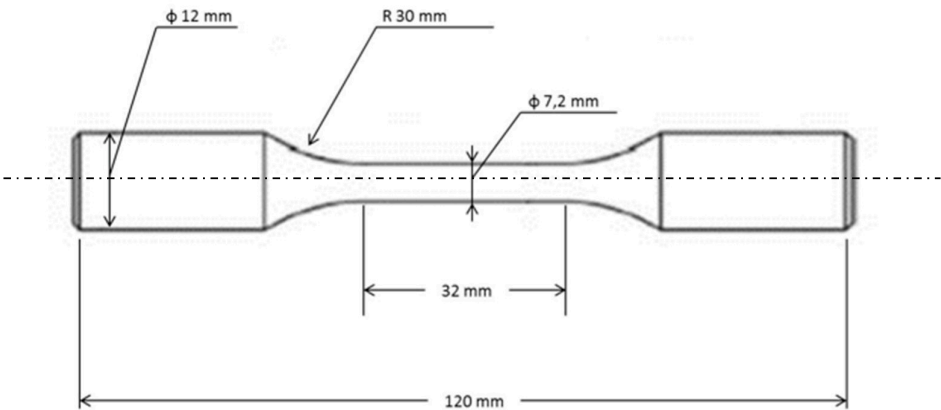
Figure 1. Geometry of rotating bending fatigue specimens

Subsequently, they were finished with emery papers in order to achieve two different surface roughness values, Ra=0.6-0.8 μm (samples abbreviation S0.8) and Ra=0.2-0.3 μm (samples abbreviation S0.3). A set of T6 heat-treated specimens was surface treated by Plasma Electrolytic Oxidation (PEO) at AHC® (Germany), using a proprietary production process (MAGOXID-COAT®). After PEO, they were sandblasted to a final surface roughness Ra=1.9÷2.1 μm (sample abbreviation SP). Surface roughness was checked by a stylus profilometer (tip radius: 5 μm).

Fatigue tests were carried out on samples with two different Ra values that represent the typical surface finishing applied to magnesium components for high performance applications. The PEO treatment, instead, is often applied to components that need high mechanical properties combined with good corrosion resistance and less strict dimensional and roughness requirements. These components, for example bike frames, are typically sandblasted and not machined after PEO.

The microstructure of the base and PEO treated alloy, both in surface and cross-section, was analysed by optical microscopy (OM) and Scanning Electron Microscopy (SEM) Zeiss EVO® equipped with an Energy Dispersive Spectroscopy (EDS) (Oxford INCA 350) microprobe.

Microstructural characterisation was carried out on samples prepared by standard metallographic techniques (grinding with SiC emery papers 800, 1200, 2000 grit; polishing with diamond 9, 3, 1 μm) and chemically etched with Nital 2 (HNO_3 2% vol. with ethanol). Image analyses on the optical micrographs (OM) were carried out using the ®Image Pro-Plus software and grain size was evaluated using the linear intercept method, according to ASTM E112-10 [32].

The adhesion/cohesion of the PEO layer was evaluated by the scratch test method, using a Revetest system (CSM Instruments SA, Switzerland) equipped with a diamond indenter (200 μm diameter). The scratch indentations were carried out using a linear progressive load mode, from 1 to 20 N, with a linear speed rate of 10 mm/min^{-1} and for a scratch length of 6 mm. The testing conditions were set based on experimental trials.

Rotating bending fatigue tests were carried out both on the untreated specimens with different surface roughness (S0.3 and S0.8 series), and on the PEO treated ones (SP series), according to UNI 3964 [33] using the staircase method, at a frequency of 90 Hz and at a stress ratio R=-1. The maximum number of cycles was set to $2x10^6$ cycles. To relate the different surface conditions to the fatigue behaviour, SEM analyses of the fracture surfaces were carried out.

3. Results and discussion

3.1 Microstructure of the untreated alloy

OM and SEM images of the EV31A-T6 alloy are reported in Fig. 2. The microstructure is composed of equiaxed grains with an average size of 45 ± 2 μm (Fig. 2a). The T6 heat treatment did not completely dissolve the ternary eutectic compound $Mg_{12}Nd_xGd_{(1-x)}$ located at the grain boundaries, as highlighted in Fig. 2b and SEM-EDS of Fig. 2c. Moreover, clusters of nanometric and micrometric Zr-Zn precipitates are clearly visible only at the grain centre, as shown by SEM-EDS analysis reported in Fig. 3 (spectra 3-5). A more detailed microstructural investigation on the strengthening precipitates, formed by the aging treatment, was reported by the authors in [34].

No solidification defects, such as gas and shrinkage porosities or oxides, which can adversely affect the fatigue behaviour of the alloy have been observed. This can be related both to the increased castability of the EV31A alloy, induced by the presence of RE, and to the optimised sand casting process used for samples production [35,36].

	At. %
O	3.02
Zn	1.56
Nd	6.3
Gd	0.83
Mg	88.25
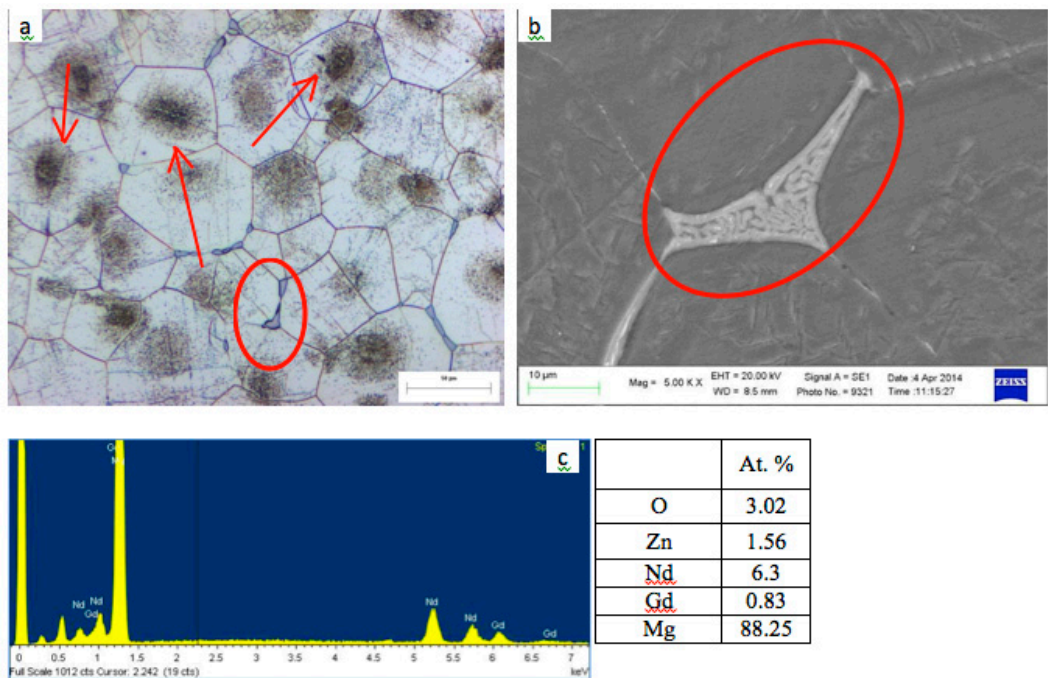
Figure 2. OM image EV31A etched with Nital2. Zr-Zn cluster and eutectic compounds highlighted respectively by red arrows and a red circles (a) and SEM image of the eutectic compound at the grain boundaries (b) with corresponding EDS analysis (c).

	At. %				
	Zn	Zr	Nd	Gd	Mg
Sp.1	0.00	0.00	0.50	0.17	99.34
Sp.2	0.00	0.34	0.47	0.21	98.98
Sp.3	0.68	1.72	0.49	0.17	96.94
Sp.4	0.35	2.97	0.47	0.00	96.21
Sp.5	0.73	1.79	0.44	0.00	97.04
Sp.6	0.00	0.33	0.53	0.24	98.90
Sp.7	0.00	0.00	0.48	0.14	99.37
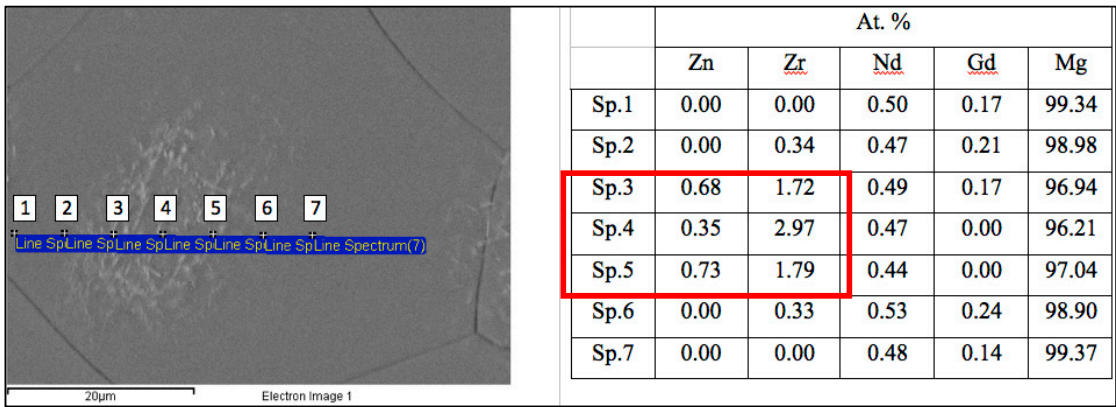
Figure 3. SEM image and EDS analyses in different points inside a grain. Zr-Zn intermetallic precipitates are located at the grain core, as shown by EDS results in spots 3,4,5.

3.2 Microstructure of the PEO-treated alloy

The PEO process was carried out by AHC® (MAGOXID-COAT®) in a saline electrolyte solution. During the process, a high voltage between the anode and the sample was generated, inducing micro-discharges on the specimen surface and converting the alloy surface into a hard oxide layer (the chemical composition of the bath and the parameters of the process are proprietary and can not be disclosed). PEO layers on Mg alloys can be usually divided into two or three regions, according to the operative treatment conditions: (i) a thin barrier layer (generally hundreds of nanometres) at the interface with the base material; (ii) a compact intermediate inner layer, with a small amount of porosities and cavities; (iii) an outer region with a high number of pores and crater density [37–39].

SEM images on the outer surface of the PEO treated and sandblasted fatigue samples are shown in Fig. 4. The sandblast process led to a relatively smooth surface, with a significant reduction of the typical cracks and microcracks present on the outer surface of the PEO layer. However, some small cracks through the pores are still present, as shown at higher magnification in Fig. 4-b.
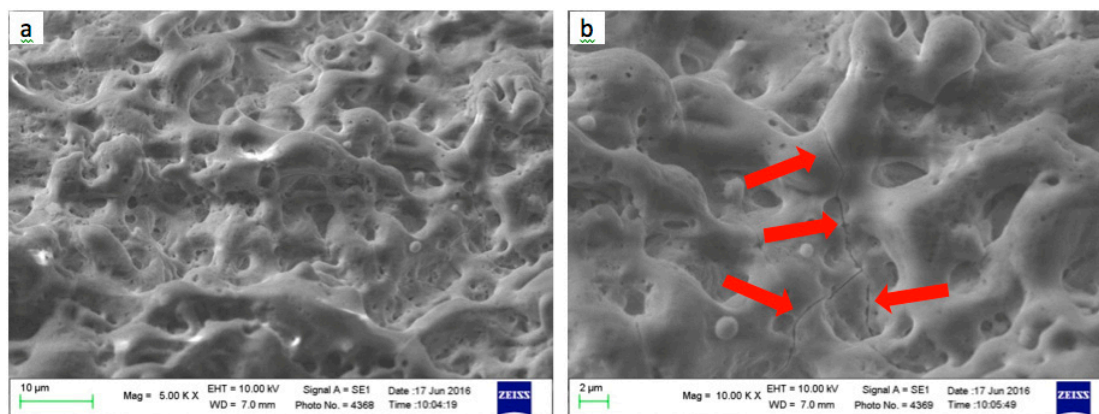
Figure 4. SEM images at different magnification of the surface of PEO treated and sandblasted fatigue specimens: smooth surface (a) with very few small cracks through the pores (b).

Representative SEM micrographs of the cross-section of the PEO-treated alloy are reported in Fig. 5 a-b. The conversion layer was about 23±3 μm in thickness and appears uniform and compact, with low density of pores and cracks, thus confirming that the sandblasting process was effective in removing the outer region of the PEO layer.
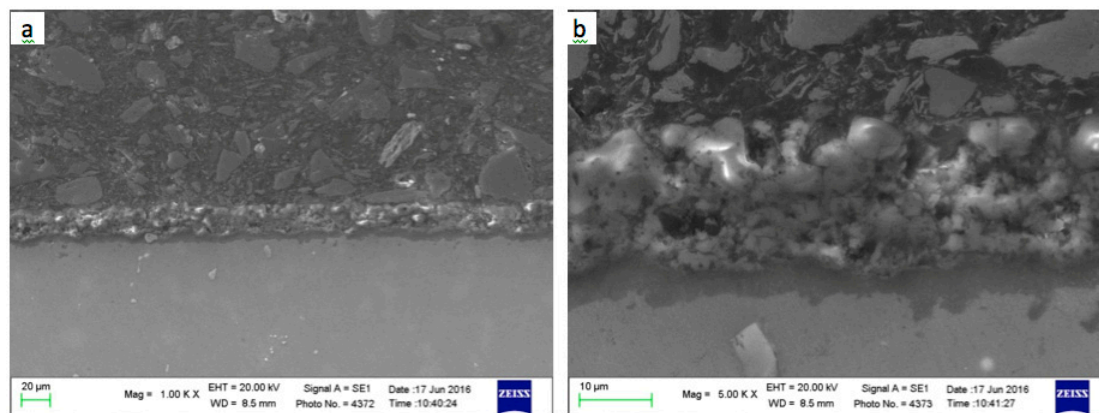
Figure 5. SEM images of PEO layer cross-section.

SEM-EDS element maps on the cross-section, shown in Fig 6, revealed a homogenous distribution of phosphorous, potassium and oxygen due to the phosphate, silicate and potassium fluoride present in the electrolytic bath. A thin fluorine-rich layer at the interface between the PEO layer and substrate can also be detected. According to [37], this layer consists of MgF_2 and plays an important role during the PEO process, reducing electrolyte conductivity, thus decreasing the working voltage. Moreover, fluoride addition helps to obtain a more compact layer, reducing porosity and correspondingly improving mechanical performance, tribological behaviour and corrosion resistance [40].
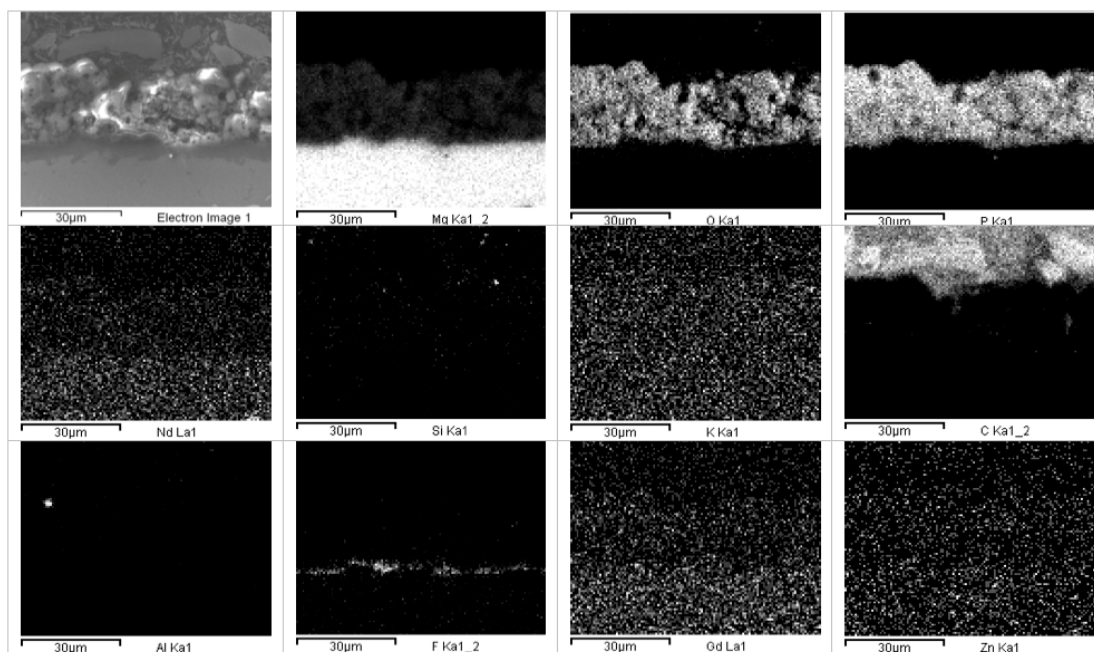
Figure 6. SEM-EDS cross section maps of the PEO layer.

3.3. Adhesion of the coating

PEO treatment on Mg alloys could be classified as a hard coating on a softer substrate material [41]. Scratch testing is a commonly used method to evaluate the adhesion of thin hard coatings. Failure depends on both substrate and coating properties, namely hardness and microstructural characteristics. A representative image of a scratch test performed on the PEO treated EV31A alloy is shown in Fig. 7a at a relatively low magnification, whereas more detailed images of the failure induced by the scratches are reported in Fig. 7b.
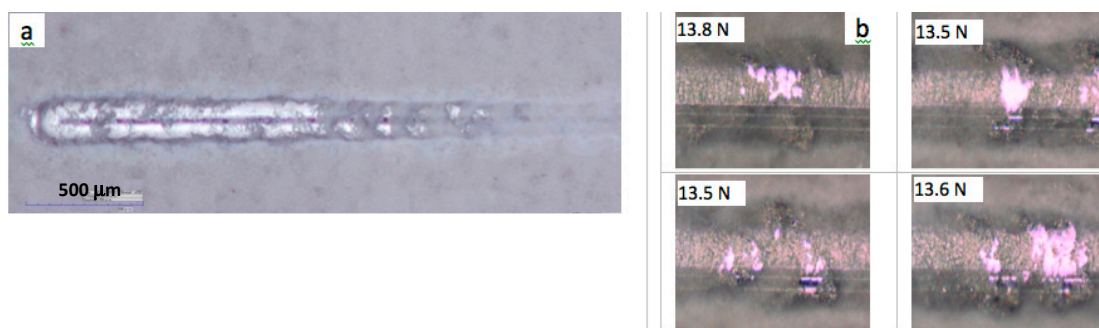
Figure 7. OM scratch test image (a); OM images of the failure area for different scratch tests with corresponding failure load (b).

Reproducible results, in terms of failure mode and critical load, were obtained. SEM images at different magnifications of a representative scratch are shown in Fig. 8a-b, with corresponding EDS X-ray maps in Fig. 9. Buckling and spallation failure are both present in Fig. 8a-b, where coating detachment from the substrate can be clearly seen.
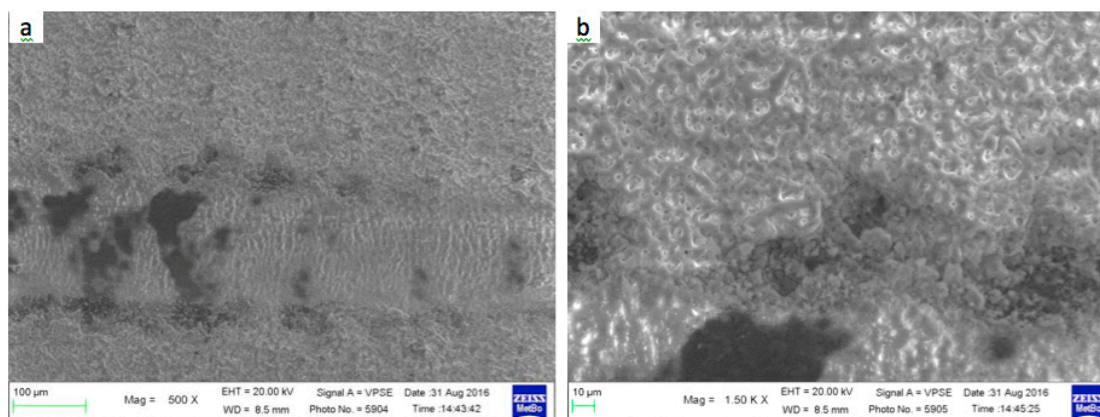
Figure 8. SEM images of the scratch test track at different magnification.
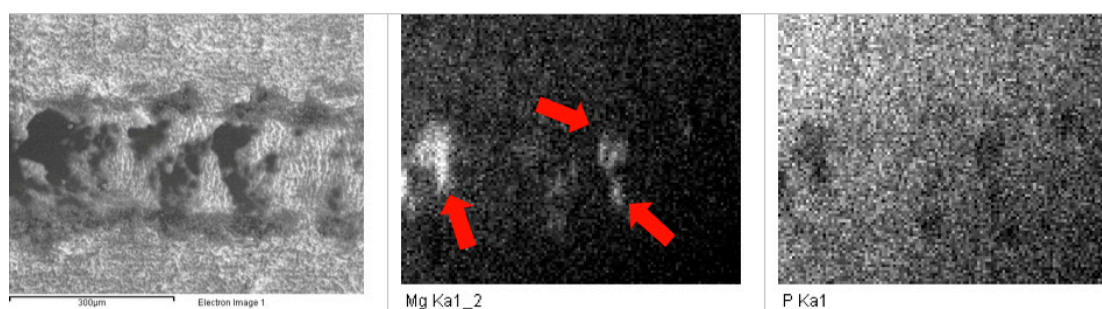
Figure 9. Representative SEM-EDS maps of the scratch tests, with the substrate highlighted by red arrows.

The EDS maps confirmed adhesion failure of the PEO coating, since the Mg substrate was detected at the bottom of the scratch, as shown in Fig. 9. Buckling failure occurs in response to the compressive stresses generated ahead of the moving indenter and typically occurs for a coating thickness less than 10 μm. Spallation occurs due to compressive shear stresses ahead of the indenter through the coating, resulting in crack nucleation that could propagate through the thickness. The continued forward motion of the indenter leads to an interfacial crack and consequent coating failure [41]. Also in this case, where the PEO layer is about 20 μm and the EV31A substrate is relatively soft, buckling and spallation are the main failure modes.

3.4 Fatigue tests

The results of the rotating bending fatigue tests carried out on the untreated sand cast EV31A Mg alloy with different surface roughness (S0.3 and S0.8 samples), and on the PEO-treated alloy are reported in Figure 10 and Table 2. It can be noted that the effect of surface roughness on the base alloy was negligible, since the difference in the mean fatigue strength values for the S0.8 and S0.3 samples was within 2% (103 and 101 MPa, respectively) and, as shown by the stair-case results in Fig. 10, the minimum stress level at which no failure occurred was 80 MPa.

The investigated alloy displayed a fatigue behaviour comparable or even better than that of other rare earth rich sand cast magnesium alloys; in fact, a fatigue strength of 98 MPa was measured on the AM-SC1 alloy (Mg -1.7wt% Nd - 1.0wt% other RE - 0.5wt% Zn - 0.5wt% Zr) [42], while the NZ30K2 alloy (Mg-2.8wt% Nd-0.19wt% Zn 0-0.50 wt% Zr) [12] showed a fatigue strength of 84 MPa (15% lower compared to that measured on the present alloy). It is also worth noting that the fatigue strength of the EV31A alloy used in the present study is also comparable with that of the most common wrought magnesium alloy AZ31 [43]. Fatigue data for several wrought and cast magnesium alloys are reported in Table 3.
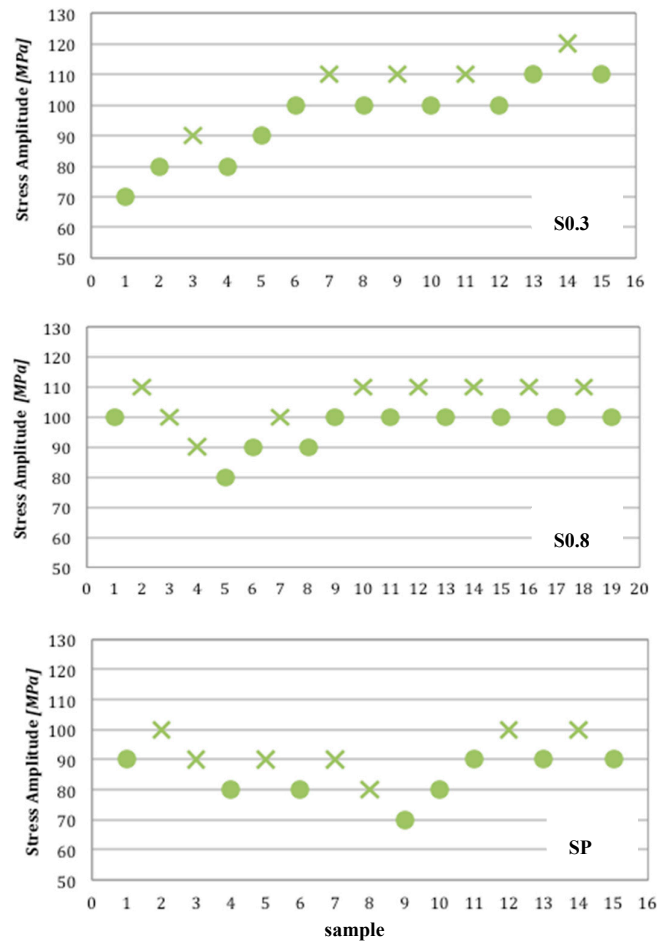
Figure 10. Stair case data for: S0.3, S0.8 and SP series (X Failures, O Survivals) . Tests were carried out according to UNI 3964 [33].

Table 2. Results of the rotating bending fatigue tests carried out according to UNI 3964 [33]. $\sigma_{D[50\%]}$ is the mean fatigue strength value (50% probability of failure), SD is the Standard Deviation.

Sample series	S0.3	S0.8	PEO
$\sigma_{D[50\%]}$ **[MPa]**	101	103	88
SD [MPa]	12	17	13

The excellent fatigue response shown by the investigated alloy in respect to the traditional cast magnesium alloys (see Table 3) can be mainly ascribed to the reduction of solidification defects (size and amounts of porosity and inclusions), and microstructural refinement induced by RE elements [7,11,12]. Moreover, it can be also related to a careful control of the sand casting process. In fact, no solidification defects were detected close to the free surface of the samples, which experiences the maximum stresses, or in the bulk.

Plasma electrolytic oxidation only induced a slightly negative effect on the fatigue performance of the EV31A Mg alloy. In fact the SP samples showed a mean fatigue strength of 88 MPa, that is about 15% lower by comparison to that of S0.3 and S0.8 (103 and 101 MPa, respectively). Moreover, in SP samples the minimum stress level at which no failure occurred was equal to 70 MPa, instead of 80 MPa for S0.3 and S0.8 samples (Fig. 10). However, by taking into account the standard deviation, the fatigue strength of bar and PEO treated alloy appeared to be comparable.

Table 3. Fatigue strength of cast and wrought magnesium alloys (literature data). * Ultrasonic fatigue test

Alloy	Fatigue Strength [MPa]	Heat Treatment	Cycles
Mg–9 wt% Al–0.8 wt% Zn-0.2 wt% Mn [1]	65	Sol. 415°C – 8h Aging 180°C - 24h	10^7
Mg–3 wt% Nd–0.2 wt% Zn– 0.45 wt% Zr [1]	87	Sol. 540°C -10h Aging 200°C - 14h	10^7
Mg-3.5 wt% Y-2.4 wt% Nd-0.5 wt% Z [8]	125	Sol. 525°C – 4h Aging 225°C - 16h	10^4
Mg–3 wt% Nd–0.2 wt% Zn–1 wt% Zr [12]	84	Sol. 540°C -10h Aging 200°C - 14h	10^7
Mg-1.7wt% Nd - 1.0wt% other RE - 0.5wt% Zn - 0.5wt% Zr [42]	98	Sol. 525°C – 8h Aging 215°C - 4h	10^7
Mg-2.9 wt% Al - 1.0 wt% Zn - 0.3 wt% Mn [43]	89	(no data reported)	10^{9*}
Mg–7 wt% Gd–5 wt% Y–1 wt% Nd–0.5 wt% Zr [44]	105	T6 (no data reported)	10^6
Mg–10 wt% Gd–3 wt% Y-0.5 wt% Zr [45]	105	Sol. 500°C – 6h Aging 225°C - 16h	10^7
Mg–9 wt% Al–0.8 wt% Zn-0.2 wt% Mn [47]	45	(no data reported)	10^{9*}
Mg–6 wt% Al–0.3 wt% Mn [47]	50	(no data reported)	10^{9*}
Mg–4 wt% Al–0.4 wt% Mn-0.9 wt% Ce [47]	42	(no data reported)	10^{9*}
Mg-2.9 wt% Al - 1.0 wt% Zn - 0.3 wt% Mn [48]	50	As rolled condition	10^7

The reduction in fatigue strength of SP samples appears to be mainly related to the intrinsic defectiveness of the ceramic conversion layer and its residual tensile stresses [41], rather than to its higher roughness. The micro-discharges, in fact, cause local melting of the surface, inducing pores and microcracks, as well as tensile stresses, during the subsequent rapid solidification [24]. Similar results were also found by Yerokhin et al. [21] who reported a fatigue strength reduction in the range of 3–10% on PEO-treated magnesium alloy rods (Mg-Al 2-Zn 1-Mn 0.2) with respect to the bare material, while A. Nemcova et al. [23] showed a 40–50% reduction in fatigue strength of PEO treated wrought AZ61 Mg alloys with respect to the untreated alloy.

3.5 Fracture surfaces analysis

It is well known that in high cycle fatigue, the crack initiation period may take up to 90% of the total fatigue life of the material, thus particular attention has been given to the crack initiation mechanisms, both in the untreated and PEO-treated alloy.

A representative SEM micrograph, at relatively low magnification, of the fracture surface of the untreated alloy is reported in Fig. 11a. The three typical regions of fatigue failure can be clearly identified: i) crack initiation; ii) crack growth; iii) final failure due to overloading.

In rotating bending fatigue tests, the surface experiences the maximum stresses, thus the cracks mainly nucleate from it. SEM image in Fig. 11b shows, at a higher magnification, the crack initiation region in the untreated alloy, where it can be clearly seen that crack nucleation occurs at the isolated facets of cleavage planes, near the free surface of the specimen. The facets are flat and smooth,

resulting from cleavage induced by the limited number of operative slip systems characteristic of HCP Mg alloys, and appear surrounded by fatigue striations. Similar crack nucleation features were observed on other magnesium alloys by Z. Li et al. [27].

The facet cleavage is due to the development of slip bands during the cycling loading, acting as stress concentration sites; thus, once the damage takes place, the crack could quickly propagate. Cleavage was observed in a large grain with a size of about 200 μm, the average grain size of the alloy being 45 ± 2 μm. Coarse grains, in fact, can easily form longer initial cracks, due to a large number of dislocations and defects, resulting in a higher probability of localised damage under cyclic loading compared to fine grains.
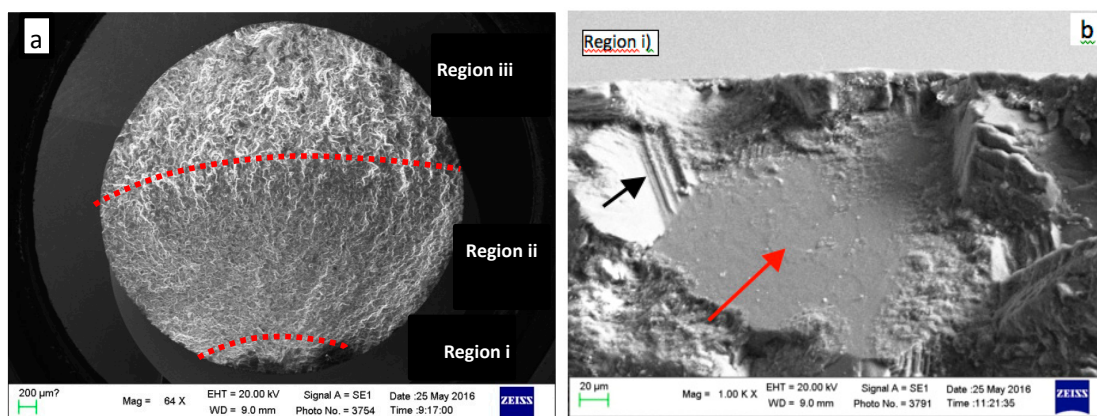
Figure 11. Representative SEM images of an untreated sample tested at 110 MPa. Typical regions of fatigue failure at low magnification: initiation (i), propagation (ii) and final failure (iii) (a); high magnification of crack initiation at isolated facets of cleavage planes (red arrow), surrounded by fatigue striations (black arrows) (b).

The PEO-treated samples showed the same crack nucleation mechanisms, as can be seen in Fig. 12 a-b, where cleavage facets and fatigue striations can be clearly identified.
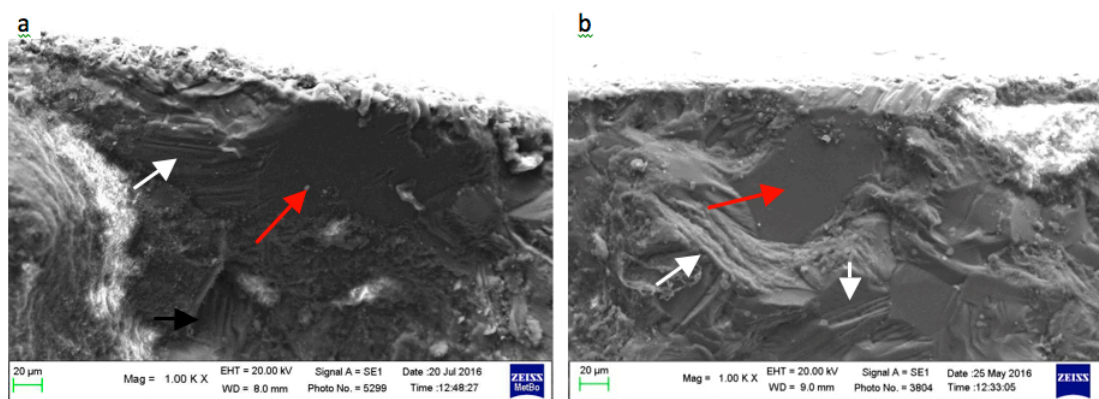
Figure 12. SEM images of crack initiation at isolated facets of cleavage planes (red arrow) surrounded by fatigue striations (white arrows) of two different PEO treated samples tested respectively at 90 MPa (a) and 100 MPa (b).

It can therefore be inferred that the lower fatigue strength of PEO treated samples is mainly due to the residual tensile stresses induced by the treatment, rather than to the defects present in the conversion layer. As previously reported, the presence of fluorine in the electrolytic bath and the sandblast process, in fact, reduced the typical solidification defects in the conversion layer (section 3.2) and consequently their influence on the fatigue behaviour of the alloy.

Representative SEM images of the crack growth region for the PEO treated and untreated samples are, instead, reported in Fig 13 a-b, showing the presence of classic fatigue striations. In Mg alloys their formation is generally associated with the dislocation slip and twinning mechanisms in the plastic zone ahead of the fatigue crack tip [4,6,48].
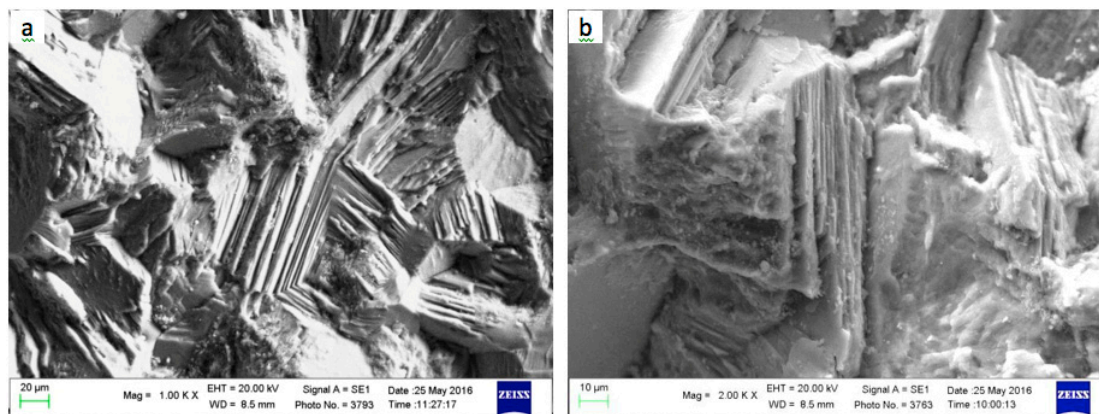
Figure 13. Representative SEM images of the crack growth region: SP sample tested at 100 MPa (a) and S0.2 sample tested at 110 MPa (b).

In this region also secondary transgranular cracks are clearly visible, as shown by representative OM images on longitudinal sections of fatigue samples (Fig. 14 a); they originated from the main cracks, confirming a transgranular and intergranular mixed mode of crack propagation. Slip bands can be clearly seen inside the grains (Fig 14 b), confirming the previously discussed mechanism for fatigue striations formation.
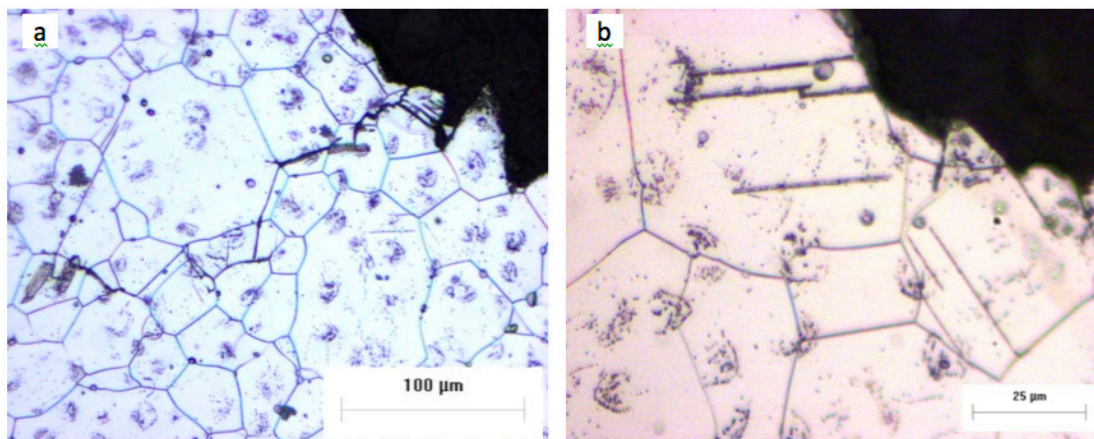
Figure 14. Representative OM images of longitudinal sections (parallel to the gauge length), of a S0.2 samples tested at 110MPa: secondary transgranular cracks (a) and slip bands inside the grains (b).

Finally, representative SEM images of the overloading regions are reported in Fig 15, where a typical brittle morphology, with cleavage planes and secondary cracks, can be observed.
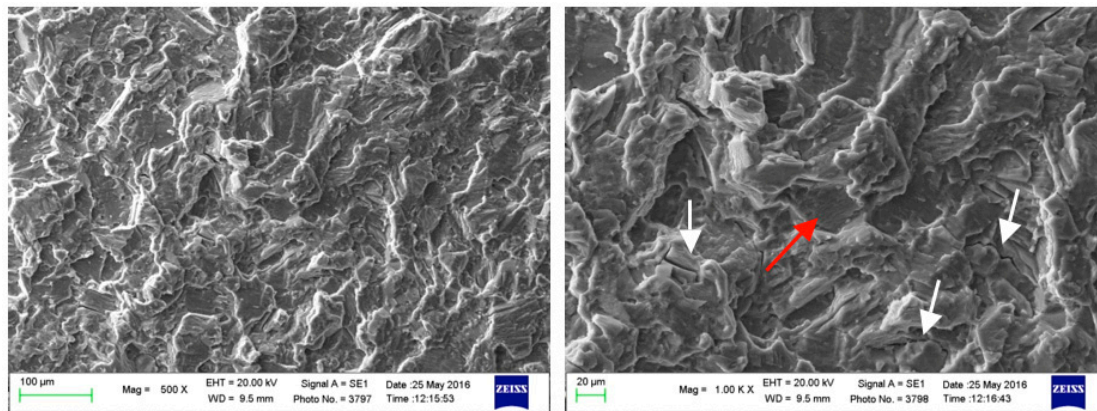
Figure 15. Representative SEM images in the overloading area at low magnification (a), and high magnification with cleavage planes (red arrow) and secondary microcracks (white arrows) (b).

4. Conclusions

The effect of surface roughness and plasma electrolytic oxidation on the fatigue behaviour of the innovative rare-earth rich sand cast EV31A Mg alloy was investigated.

The fatigue strength of the untreated alloy was comparable with that of wrought Mg alloy, also due to its chemical composition as well as to the high quality of the cast product, substantially free from solidification defects due to a well-controlled sand casting process. The effect of specimen surface roughness was negligible.

The PEO treatment caused no more than 15% reduction in the alloy mean fatigue strength. The relatively low reduction in fatigue strength was related to the compact and well adherent conversion layer. A positive effect on its fatigue behaviour was probably also induced by the sandblasting process, carried out on the PEO-treated specimens, that removed the outer layer with the largest pores, channels and craters, typically induced by plasma electrolytic oxidation.

Similar mechanisms of fatigue failure were observed in base and PEO-treated alloys, with crack nucleation sites located close to the large facets of the cleavage planes. This allows us to conclude that the observed reduction in fatigue performance was mainly induced by the residual tensile stresses due to PEO treatment in the substrate material, rather than the defects present in the conversion layer.

References

1. Li ZM, Wang QG, Luo A.A., Peng LM, Fu PH, Wang YX. Improved high cycle fatigue properties of a new magnesium alloy. *Mater Sci Eng A* **2013**, 582, 170–7.
2. Friedrich H, Schumann S. Research for a "new age of magnesium" in the automotive industry. *J Mater Process Technol* **2001**, 117, 276–81.
3. Pantelakis SG, Alexopoulos ND, Chamos A. N. Mechanical Performance Evaluation of Cast Magnesium Alloys for Automotive and Aeronautical Applications. *J Eng Mater Technol* **2007**, 129, 422.
4. Mirza FA, Chen DL, Li DJ, Zeng XQ. Cyclic Deformation Behavior of a Rare-Earth Containing Extruded Magnesium Alloy: Effect of Heat Treatment. *Metall Mater Trans A Phys Metall Mater Sci* **2014**, 46, 1168–87.
5. Li Z, Wang Q, Luo AA, Fu P, Peng L. Fatigue strength dependence on the ultimate tensile strength and hardness in magnesium alloys. *Int J Fatigue* **2015**, 80, 468–76.

6. Li Z, Wang Q, Luo AA, Fu P, Peng L, Wang Y, et al. High cycle fatigue of cast Mg-3Nd-0.2Zn magnesium alloys. *Metall Mater Trans A Phys Metall Mater Sci* **2013**, 44, 5202–15.

7. Peng L, Fu P, Li Z, Wang Y, Jiang H. High cycle fatigue properties of cast Mg-xNd-0.2Zn-Zr alloys. *J Mater Sci* **2014**, 49, 7105–15.

8. Li H, Lv F, Xiao Z, Liang X, Sang F, Li P. Low-cycle fatigue behavior of a cast Mg–Y–Nd–Zr alloy by T6 heat treatment. Mater Sci Eng A 2016, 676, 377–84.

9. Mirza FA, Chen DL. Fatigue of rare-earth containing magnesium alloys: A review. *Fatigue Fract Eng Mater Struct* **2014**, 37, 831–53.

10. Mokhtarishirazabad M, Boutorabi SMA, Azadi M, Nikravan M. Effect of rare earth elements on high cycle fatigue behavior of AZ91 alloy. *Mater Sci Eng A* **2013**, 587, 179–84.

11. Pan F, Yang M, Chen X. A Review on Casting Magnesium Alloys: Modification of Commercial Alloys and Development of New Alloys A Review on Casting Magnesium Alloys: Modification of Commercial Alloys and Development of New Alloys. *J Mater Sci Technol* **2016**, 1–11.

12. Peng LM, Fu PH, Li ZM, Yue HY, Li DY, Wang YX. High cycle fatigue behaviors of low pressure cast Mg-3Nd-0.2Zn-2Zr alloys. *Mater Sci Eng A* **2014**, 611, 170–6.

13. Wang F, Dong J, Jiang Y, Ding W. Cyclic deformation and fatigue of extruded Mg-Gd-Y magnesium alloy. *Mater Sci Eng A* **2013**, 561, 403–10.

14. Stanford N, Barnett M. Effect of composition on the texture and deformation behaviour of wrought Mg alloys. *Scr Mater* **2008**, 58, 179–82.

15. Hadorn JP, Hantzsche K, Yi S, Bohlen J, Letzig D, Agnew SR. Effects of solute and second-phase particles on the texture of Nd-containing Mg alloys. *Metall Mater Trans A Phys Metall Mater Sci* **2012**, 43, 1363–75.

16. Mirza FA, Chen DL, Li DJ, Zeng XQ. Effect of rare earth elements on deformation behavior of an extruded Mg-10Gd-3Y-0.5Zr alloy during compression. *Mater Des* **2013**, 46, 411–8.

17. E.D. Morales, E. Ghali, N. Hort, W. Dietzel, K.U. Kainer MS, 419–422 F. Corrosion behaviour of magnesium alloys with RE additions in sodium chloride solutions. *Mater Sci Forum* **2003**, 419–422, 867–72.

18. Wu G, Fan Y, Gao H, Zhai C, Zhu YP. The effect of Ca and rare earth elements on the microstructure, mechanical properties and corrosion behavior of AZ91D. *Mater Sci Eng A* **2005**, 408, 255–63.

19. Smola B, Stulı I, von Buch F, Mordike BL. Structural aspects of high performance Mg alloys design. *Mater Sci Eng A* **2002**, 324, 113–7.

20. Xiao W, Shen Y, Wang L, Wu Y, Cao Z, Jia S, et al. The influences of rare earth content on the microstructure and mechanical properties of Mg–7Zn–5Al alloy. *Mater Des* **2010**, 31, 3542–9.

21. Yerokhin AL, Shatrov A, Samsonov V, Shashkov P, Leyland A, Matthews A. Fatigue properties of Keronite coatings on a magnesium alloy. *Surf Coatings Technol* **2004**, 182, 78–84.

22. Khan SA, Miyashita Y, Mutoh Y, Koike T. Effect of anodized layer thickness on fatigue behavior of magnesium alloy. *Mater Sci Eng A* **2008**, 474, 261–9.

23. Nemcova A, Skeldon P, Thompson GE, Morse S, Cizek J, Pacal B. Influence of plasma electrolytic oxidation on fatigue performance of AZ61 magnesium alloy. *Corros Sci* **2014**, 82, 58–66.

24. Bala Srinivasan P, Liang J, Blawert C, Dietzel W. Dry sliding wear behaviour of magnesium oxide and zirconium oxide plasma electrolytic oxidation coated magnesium alloy. *Appl Surf Sci* **2010**, 256, 3265–73.

25. Liu C, Liang J, Zhou J, Li Q, Peng Z, Wang L. Characterization and corrosion behavior of plasma electrolytic oxidation coated AZ91-T6 magnesium alloy. *Surf Coatings Technol* **2016**, 304, 179–87.

26. Durdu S, Usta M. Characterization and mechanical properties of coatings on magnesium by micro arc oxidation. *Appl Surf Sci* **2012**, 261, 774–82.

27. Li Z, Wang Q, Luo A.A, Peng L, Zhang P. Fatigue behavior and life prediction of cast magnesium alloys. *Mater Sci Eng A* **2015**, 647, 113–26.

28. Liu W, Jiang L, Cao L, Mei J, Wu G, Zhang S, et al. Fatigue behavior and plane-strain fracture toughness of sand-cast Mg-10Gd-3Y-0.5Zr magnesium alloy. *Mater Des* **2014**, 59, 466–74.

29. Xu DK, Liu L, Xu YB, Han EH. The fatigue behavior of I-phase containing as-cast Mg-Zn-Y-Zr alloy. *Acta Mater* **2008**, 56, 985–94.

30. Bhuiyan MS, Mutoh Y, Murai T, Iwakami S. Corrosion fatigue behavior of extruded magnesium alloy AZ61 under three different corrosive environments. *Int J Fatigue* **2008**, 30, 1756–65.

31. International Organization for Standardization. ISO 1143 2002, **2002**.

32. ASTM E112-10 - Standard Test Methods for Determining Average Grain Size. **2012**.

33. UNI 3964 – 85, Mechanical Testing of Metallic Materials Fatigue Testing at RoomTemperature, 1985, **2010**.

34. Angelini V, Ceschini L, Morri A, Apelian D. Influence of heat treatment on microstructure and mechanical properties of rare earth rich magnesium alloy. *Int J Met Cast* **2016.** DOI 10.1007/s40962-016-0070-2

35. Lyon P. New magnesium alloy for aerospace and speciality applications. In *Magnesium Technology,* Editor Luo AA, TMS, 2004, p. 311–5.

36. Qudong W, Yizhen L, Xiaoqin Z, Wenjiang D, Yanping Z, Qinghua L, et al. Study on the fluidity of AZ91+xRE magnesium alloy. *Mater Sci Eng A* **1999**, 271, 109–15.

37. Duan H, Yan C, Wang F, Effect of electrolyte additives on performance of plasma electrolytic oxidation films formed on magnesium alloy AZ91D. Electrochimica Acta, 2007, 52, 3785–3793

38. Arrabal R, Matykina E, Hashimoto T, Skeldon P, Thompson GE. Characterization of AC PEO coatings on magnesium alloys. *Surf Coatings Technol* **2009**, 203, 2207–20.

39. Ko YG, Namgung S, Shin DH. Correlation between KOH concentration and surface properties of AZ91 magnesium alloy coated by plasma electrolytic oxidation. *Surf Coatings Technol* **2010**, 205, 2525–31.

40. Blawert C, Srinivasan PB. In *Surface engineering of light alloys* 1st ed.; Editors Hanshan Dong, Woodhead Publishing UK, **2010**, pp 155-180.

41. Bull SJ, G.-Berasetegui E. An overview of the potential of quantitative coating adhesion measurement by scratch testing. *Tribol Interface Eng Ser* **2006**, 51, 136–65.

42. Li Z, Fu P, Peng L, Becker EP, Wu G. Influence of solution temperature on fatigue behavior of AM-SC1 cast magnesium alloy. *Mater Sci Eng A* **2013**, 565, 250–7.

43. Yang F, Yin SM, Li SX, Zhang ZF. Crack initiation mechanism of extruded AZ31 magnesium alloy in the very high cycle fatigue regime. *Mater Sci Eng A* **2008**, 491:131–6.

44. Wang SD, Xu DK, Wang BJ, Han EH, Dong C. Effect of corrosion attack on the fatigue behavior of an as-cast Mg-7%Gd-5%Y-1%Nd-0.5%Zr alloy. Mater Des 2015, 84, 185–93.

45. Liu WC, Dong J, Zhang P, Korsunsky AM, Song X, Ding WJ. Improvement of fatigue properties by shot peening for Mg-10Gd-3Y alloys under different conditions. Mater Sci Eng A 2011, 528, 5935–44.

46. Mayer H, Papakyriacou M, Zettl B, Stanzl-Tschegg S.E. Influence of porosity on the fatigue limit of die cast magnesium and aluminium alloys. *Int J Fatigue* **2003,** 25, 245–256.

47. Tokaji K, Kamakura M, Ishiizumi Y, Hasegawa N. Fatigue behaviour and fracture mechanism of a rolled AZ31 magnesium alloy. *Int J Fatigue* **2004,** 26, 1217–1224

48. Begum S, Chen DL, Xu S, Luo AA. Effect of strain ratio and strain rate on low cycle fatigue behavior of AZ31 wrought magnesium alloy. *Mater Sci Eng A* **2009**, 517, 334–43.